Linear viscoelastic behavior of dense hard-sphere dispersions

J. C. van der Werff and C. G. de Kruif
Van't Hoff Laboratory, University of Utrecht, Padualaan 8, 3584 CH Utrecht, The Netherlands

C. Blom and J. Mellema
Rheology Group, Department of Applied Physics, Twente University of Technology, 7500 AE Enschede, The Netherlands
(Received 6 July 1988)

The complex shear viscosity of sterically stabilized colloidal dispersions of different-sized silica particles (radius $a=28-76$ nm) was measured with torsion resonators and a nickel-tube resonator between 80 Hz and 200 kHz. The volume fraction of the samples was varied from 0.10 to 0.60. In the intermediate-frequency region, the real and the imaginary parts of the complex shear viscosity decay as $\omega^{-1/2}$ to their limiting values. The viscoelastic behavior can be described in terms of one relaxation strength G_1 and a series of relaxation times with $\tau_p=\tau_1 p^{-2}$. The complex shear viscosity scales with the dimensionless relaxation strength $a^2G_1/D_0\eta_s$, the dimensionless relaxation time $D_0\tau_1/a^2$, and the dimensionless angular frequency $a^2\omega/D_0$. The dimensionless groups $a^2G_1/D_0\eta_s$ and $D_0\tau_1/a^2$ are a function of the volume fraction only. At higher volume fractions the high-frequency limiting values of the real part of the complex shear viscosity, η'_∞, corroborate values calculated by Beenakker [Physica **128A**, 48 (1984)].

I. INTRODUCTION

The macroscopic rheological properties of dispersions can be ascribed to the interplay of colloidal and fluid-mechanical interactions. On a microscopic scale, these interactions determine the structure of the dispersion, i.e., the local degree of particle (dis)order.

Stable colloidal dispersions often display clear viscoelastic behavior. In particular, dispersions of particles with strong electrostatic repulsions have been the subject of many studies.[1,2] In these dispersions, the viscoelasticity originates from the interparticle forces. In equilibrium, the structure is such that the free energy of the particle interaction is at a minimum. When the dispersion is strained, the electrostatic energy increases. When the strain stops, this higher free-energy state drives the system through relaxation towards the equilibrium configuration.

Weakly flocculated dispersions are another type of dispersions which display viscoelasticity.[3,4] The shear deforms the flocs and the free energy increases since the particles that build up the flocs are displaced out of their equilibrium positions. In these types of dispersions, it is the direct interaction between the particles that mediates the free-energy storage.

Of course, a change in the relative positions of strongly interacting particles is not the only cause of viscoelasticity. In microemulsions, the particles themselves can be deformed by the strain.[5,6] The surface area of the particles becomes larger during the deformation. The resulting increase in surface free energy of the particles leads to a storage of free energy and explains the viscoelasticity.

As we will show in this paper, there is still another cause of viscoelasticity. We demonstrate this by presenting measurements on hard-sphere dispersions. In equilibrium, the supramolecular fluid attains a liquidlike order. Perturbations from the equilibrium structure will be driven back to equilibrium. It is simply the change in configurational free energy that is responsible for the viscoelasticity. In equilibrium, the particle distribution is determined by Brownian motion. If the dispersion is weakly strained in a slow oscillatory motion, the equilibrium distribution is disturbed and as a result the entropy decreases (the free energy increases). The Brownian motion rerandomizes the dispersion. During the diffusion of the individual particles, free energy is dissipated. At intermediate and high frequencies there is no time for the equilibrium to be restored during the oscillations; free energy is stored in the medium by virtue of the distorted configuration of the particles and viscoelastic behavior is observed. Under a high-frequency strain, the distribution does not relax and no free energy is dissipated via relaxation. The dispersion therefore behaves in a "Newtonian" way and the high-frequency limit of the complex shear viscosity is determined purely by hydrodynamics.

In previous studies[7,8] it was shown that the equilibrium properties of dispersions of sterically stabilized silica spheres dispersed in cyclohexane closely resemble those of the hard-sphere system. Light and neutron scattering studies showed that the compressibility, which is proportional to the inverse of the structure factor $S(K)$ at zero wave vector $[S^{-1}(K=0)]$ and the structure factor $S(K)$ itself agree with the Percus-Yevick solution of the radial distribution function $g(r)$ for hard spheres.

The steady-shear viscosity of these dispersions was measured as a function of particle size, shear rate, and volume fraction.[9,10] It was found that the properties of these dispersions were in agreement with the theoretical results developed by Einstein[11] and Batchelor[12-14] for (dilute) hard-sphere dispersion. The fundamental scaling properties as predicted by exact theory (and more intui-

tively by Krieger[15] were present. The study was not limited to dilute dispersions, but we were able to determine the relevant rheological parameters up to the volume fraction $\phi=0.60$.

In this study we analyze measurements of the linear viscoelastic behavior of the hard-sphere silica systems. The complex shear viscosity is measured as a function of particle size, volume fraction, and frequency. It is an extension of the experiments that were reported in Ref. 16.

The main advantage of our hard-sphere dispersion is the fact that with it is experimentally possible to vary particle size and volume fraction without influencing the interaction potential. In previous studies, we showed the scaling parameters in the steady-shear viscosity; we are now able to determine the scaling properties of the complex shear viscosity.

In Sec. II we will show that basic scaling behavior can be deduced from a theory worked out by Batchelor.[14] The experiments will be discussed in this context. Further, we will relate our experimental results to the theory of Russel and Gast[17] which is an extension of Batchelor's concept. The high-frequency limit of the real part of the complex shear viscosity η'_∞ will be compared with calculations by Beenakker[18] and by Russel and Gast.

II. THEORY

A. Theoretical background

The viscoelastic behavior of a dispersion of hard spheres in a Newtonian fluid arises from the disturbance of the particle distribution function $P(\{\mathbf{r}\},t)$, which is a function of all position coordinates of the Brownian particles and time. When the equilibrium particle distribution is disturbed by shear, it relaxes by Brownian motion. The competition between shear and Brownian motion can be expressed in the so-called Peclet number $a^2\dot{\gamma}/D_0$, where a is the particle radius, $\dot{\gamma}$ is the shear rate, and D_0 is the Stokes-Einstein diffusion coefficient, $D_0=k_BT/6\pi\eta a$ (k_B is the Boltzmann constant, T is the absolute temperature, and η is the shear viscosity). This dimensionless quantity determines the rate of distortion of the (pair) distribution function and is the important parameter in many non-Newtonian phenomena encountered in dispersion rheology.[9,10,14–17]

The particle distribution function plays an important role in the calculation of the stress that is generated in a dispersion by an external force field. Such a calculation contains an ensemble averaging [thus an averaging over $P(\{\mathbf{r}\},t)$] over the stress generated in a dispersion in which the particles are held in fixed positions.[12]

When an oscillatory flow is imposed on a dispersion, the distortion of the distribution function is as a result partly in phase with the velocity and partly out of phase. The disturbed pair distribution function can thus be represented as a complex quantity. In turn, this leads to a complex shear viscosity $\eta^*(\omega)$,

$$\eta^*(\omega)=\eta'(\omega)-i\eta''(\omega) . \tag{1}$$

The real part of the complex shear viscosity is in phase with the applied rate of shear and is a dissipative term. The imaginary part is related to the free-energy storage.

Batchelor assumed a regular expansion of the pair distribution function $g(r)$ in the Peclet number $a^2\dot{\gamma}/D_0$. For low Peclet numbers, thus for dominant Brownian motion, and for small strains, the distribution function which is disturbed by an oscillating flow can be written as[14]

$$g=g_0\left[1-\frac{a^2\boldsymbol{\rho}\cdot\dot{\underline{E}}\cdot\boldsymbol{\rho}}{2D_0\rho^2}fe^{i\omega t}\right] , \tag{2}$$

where ρ is a dimensionless distance ($\rho=r/a$), $\dot{\underline{E}}$ is the rate of strain tensor, g_0 is the equilibrium pair distribution function, and f is a hydrodynamic function. In an oscillating flow field, f is complex.[17] In this section we shall calculate the relaxation time of the pair distribution function from Batchelor's theory. In this calculation, we implicitly assume that the expansion given by Eq. (2) is correct.[19]

To calculate the relaxation time, we need to use some results of Batchelor and Green who developed an extensive theory for the evaluation of the bulk stress in a semidilute suspension of hard spheres.[13] Calculations in which they neglected Brownian motion and in which a random particle distribution was assumed [in this case $g(r)=1$] led to the following result for the relative viscosity η_r:

$$\eta_r=\eta/\eta_s=1+2.5\phi+5.2\phi^2 , \tag{3}$$

where η_s is the solvent viscosity and ϕ is the volume fraction. This result can be regarded as the high-frequency value of the real part of the complex shear viscosity, η'_∞.

If Brownian motion is taken into account, then an extra term to describe the extra stress generated in the dispersion by the random movements of the particles has to be added to Eq. (3). Batchelor[14] calculated for this extra stress term $\underline{\Sigma}^B$

$$\underline{\Sigma}^B=\tfrac{9}{20}\eta_s\phi^2\dot{\underline{E}}\int_2^\infty\rho^2W(\rho)g_0f\,d\rho+\underline{P} , \tag{4}$$

where $\underline{P}$ represents a pressure term. In equilibrium, $f=0$ and the Brownian motion generates only an osmotic pressure. $W(\rho)$ is a function governed by the hydrodynamics. Numerical evaluation of the integral contributes $0.97\phi^2$ to the relative viscosity, leading to

$$\eta_r=\eta/\eta_s=1+2.5\phi+(5.2+0.97)\phi^2 . \tag{5}$$

In this result, η_r is the low-shear and zero-frequency value η'_0 for the viscosity of a hard-sphere dispersion because in the calculation Brownian motion dominates and the shear field is a steady one (f is real).

At infinite angular frequency, the affine distortion of the distribution function is responsible for the free-energy storage. For the calculation of $\eta'(\omega)$, we have to replace f in Eq. (4) by the imaginary part f''. The high-frequency value of f'' was implicitly given by Batchelor,[17]

$$f''(\omega\rightarrow\infty)=(2D_0/a^2\omega)W(\rho) , \tag{6}$$

and we find that

$$G'_\infty = \lim_{\omega\to\infty} \omega\eta'' = \tfrac{9}{20}(D_0/a^2)\eta_s\phi^2\int_2^\infty \rho^2 W^2(\rho) g_0 d\rho$$
$$= 3.9\phi^2 D_0\eta_s/a^2 , \quad (7)$$

where we used $g_0=1$. If we further assume that the decrease of the real part of the complex shear viscosity with increasing frequency is due to the vanishing contribution of Brownian motion, and that the relaxation mechanism can be described with a single relaxation time, then we can calculate the relaxation time as follows:

$$\tau=(\eta'_0-\eta'_\infty)/G'_\infty = \tfrac{0.97}{3.9}a^2/D_0 = 0.25a^2/D_0 . \quad (8)$$

The result Eq. (8) can only be applied to semidilute dispersions ($\phi<0.10$) because only (hydrodynamic) pair interactions were taken into account and the particle distribution was assumed to be random. Experiments in this concentration range show that the viscoelastic effects are too small to be measured and therefore no direct comparison can be made with the result given in Eq. (8). However, the predicted dependence of τ on the ratio a^2/D_0 is important.

Russel and Gast[17] extended Batchelor's theory. They include many-particle interactions by means of the potential of mean force $V_{\rm mf}$ which is related to $g(r)$ as

$$V_{\rm mf} = -k_B T \ln g(r) . \quad (9)$$

The particle interactions that determine the structure of the pair distribution function (or radial distribution function) give rise to a potential of mean force, which Russel and Gast treat as an effective direct interaction potential. In the Russel-Gast theory the hydrodynamics are still treated at the pair level. In Sec. IV it is shown that measurements on hard-sphere dispersions show a measurable frequency-dependent viscosity in the volume fraction range $0.30<\phi<0.60$. We were not able to perform measurements on samples with $\phi>0.60$. For the concentrated dispersions, we calculate a relaxation time from the Russel-Gast theory. From the Figs. 3 and 6 in Ref. 17 one can calculate the single relaxation time τ which is defined by Eq. (8). Between $0.35<\phi<0.55$, the coefficient of a^2/D_0 in τ varies from 0.10 to 0.02. (Note that these numbers differ by a factor of 2 from those that we reported in Ref. 16. This is due to an error in Fig. 6 in Ref. 17; the values for G'_∞ are a factor of 2 too large (erratum supplied by W. B. Russel and A. P. Gast). This implies that the particle distribution relaxes faster in more concentrated dispersions, which is in contradiction with the experimental results (see Sec. IV B).

In Sec. IV we shall show that the timescale of the diffusion process that is responsible for the relaxation is a time scale between the short-time self-diffusion time scale and the time scale of long-time self-diffusion. Collective diffusion is not relevant since in the dispersion there is no macroscopic concentration gradient present to drive such a collective diffusion process. The short-time self-diffusion process is thought to be the diffusion of a particle within a cage of surrounding particles. The other limit, the long-time self-diffusion, is the diffusion of a single (tracer) particle over larger distances. Interpretation of the data (see Sec. IV) suggests that the longest relaxation time corresponds to a diffusion process which is somewhere in between these limits, e.g., the diffusion from one cage into another. It would therefore be interesting to replace the diffusion coefficient at infinite dilution (D_0) in the expression for τ by the self-diffusion constant D_s that belongs to the time scale of the longest relaxation time. Unfortunately, no complete data are yet available. From both theoretical[20,21] and experimental[22,23] studies it is known that $D_s^{\rm short}$ decreases with increasing volume fraction. $D_s^{\rm long}$ shows a similar behavior, but at higher volume fractions ($\phi=0.45$), the long-time mobility is almost zero[24] whereas the short-time diffusion is only decreased by a factor of 3 with respect to the free diffusion. At this volume fraction the system still relaxes fast, which implies that the diffusion process is more closely related to short-time self-diffusion than to long-time self-diffusion. We therefore replace D_0 by $D_s^{\rm short}$. Up to $\phi=0.45$, reliable numbers are available for $D_s^{\rm short}$. At $\phi=0.45$, $D_s^{\rm short}=0.3D_0$, leading to $\tau=0.8a^2/D_0$.

It is tempting to interpret the theory of Batchelor and Green and Russel and Gast in such a way that a single relaxation time is obtained. This implies that the viscoelastic behavior of a hard-sphere colloidal dispersion can be described by a single relaxation mechanism. The theory itself says nothing about the number of relaxation processes. The experiments to be reported here show that we need a series of relaxation times to describe the experimental results. We expect that when interactions are described at the pair level, the relaxation time is a function of the interparticle separation. The theory, however, does not allow for a straightforward interpretation that leads to expressions for all relaxation times. With Eq. (8) we calculated a "mean" relaxation time since we averaged over all particle pair positions while the positions of all the other particles are randomized.

B. Theoretical predictions for η'_∞

The high-frequency limit of the real part of the complex shear viscosity was among others[25–28] calculated by Beenakker.[18] Beenakker solves the Navier-Stokes equation for a dense suspension of hard spheres. The effects of Brownian motion are neglected. Harmonically oscillating forces act on the particles that are distributed according to the Percus-Yevick equilibrium distribution. Beenakker gives a lower- and an upper-frequency limit for measurements that can be compared with his calculations. The upper limit is determined by the frequency at which inertia effects become important. At frequencies lower than the lower limit, Brownian motion cannot be neglected. For our model system the data that can be compared with Beenakker's calculations have to be recorded in the frequency interval 10^4–10^8 rad/s.

Russel and Gast[17] calculate η'_∞ also. They use Batchelor's formalism that leads to the result given by Eq. (3) but extend the applicability of the formalism by using the equilibrium $g(r)$ as a function of volume fraction. The values of η'_∞ are lower than those obtained by Beenakker and Mazur, which clearly illustrates the importance of the many-body hydrodynamics.

C. Viscoelastic models

Since our results clearly show that a description of the complex shear viscosity in terms of a single relaxation time is inadequate, we write the complex shear viscosity as[29]

$$\eta^*(\omega)=\eta'_\infty+\sum_{p=1}^{N}\frac{G_p\tau_p}{1+i\omega\tau_p}\ , \tag{10}$$

where N is the number of relaxation processes involved. The real and imaginary parts of the complex shear viscosity are given by

$$\eta'(\omega)=\eta'_\infty+\sum_{p=1}^{N}\frac{G_p\tau_p}{1+\omega^2\tau_p^2}\ , \tag{11}$$

$$\eta''(\omega)=\sum_{p=1}^{N}\frac{\omega G_p\tau_p^2}{1+\omega^2\tau_p^2}\ , \tag{12}$$

where η'_∞ is the real part of the complex shear viscosity in the limit $\omega\rightarrow\infty$. G_p is the relaxation strength of the relaxation process with relaxation time τ_p. In the description of a relaxation process with only one relaxation time, the high-frequency tail of $[\eta'(\omega)-\eta'_\infty]$ decays as ω^{-2} and $\eta''(\omega)$ decays as ω^{-1}. In the experimental section (Sec. IV) it will be shown that both $[\eta'(\omega)-\eta'_\infty]$ and $\eta''(\omega)$ decay as $\omega^{-1/2}$.

Is is well known that such a frequency behavior can be modeled by assuming that the pth relaxation time is related to the longest relaxation time τ_1 as

$$\tau_p=\tau_1 p^{-\alpha},\quad \alpha=2 \tag{13}$$

$$G_p=\text{const}=G_1\ . \tag{14}$$

This would imply that all relaxation times are a function of a^2/D_0. Following this line, it becomes feasible to plot the complex shear viscosity as a function of the dimensionless frequency $a^2\omega/D_0$. In view of (8) we expect G_1 to be proportional to $\eta_s D_0/a^2$. The assumptions we made lead to the expressions

$$\eta'(\omega)=\eta'_\infty+\sum_{p=1}^{N}\frac{G_1\tau_1 p^2}{p^4+\omega^2\tau_1^2}\ , \tag{15}$$

$$\eta''(\omega)=\sum_{p=1}^{N}\frac{\omega G_1\tau_1^2}{p^4+\omega^2\tau_1^2}\ . \tag{16}$$

Equations (15) and (16) have the observed intermediate frequency behavior. It can be shown that at intermediate frequencies, $1\ll\omega\tau_1\ll N^2$, Eqs. (15) and (16) can be rewritten (for $\tau_p=\tau_1 p^{-\alpha}$) as

$$\eta'(\omega)-\eta'_\infty=G_1\tau_1^{1/\alpha}\omega^{-1+1/\alpha}\frac{1}{\alpha-1}\int_0^\infty\frac{dy}{1+y^{2\alpha/(\alpha-1)}}\ ,$$

$$y=(\omega\tau_1)^{1-1/\alpha} \tag{17a}$$

$$=\frac{\pi}{2\alpha\cos(\pi/2\alpha)}G_1\tau_1^{1/\alpha}\omega^{-1+1/\alpha} \tag{17b}$$

$$=1.11G_1\tau_1^{1/2}\omega^{-1/2}\quad\text{for }\alpha=2\ , \tag{17c}$$

$$\eta''(\omega)=G_1\tau_1^{1/\alpha}\omega^{-1+1/\alpha}\frac{1}{\alpha-1}\int_0^\infty\frac{y^{\alpha/(\alpha-1)}}{1+y^{2\alpha/(\alpha-1)}}dy\ ,$$

$$y=(\omega\tau_1)^{1-1/\alpha} \tag{18a}$$

$$=\frac{\pi}{2\alpha\sin(\pi/2\alpha)}G_1\tau_1^{1/\alpha}\omega^{-1+1/\alpha} \tag{18b}$$

$$=1.11G_1\tau_1^{1/2}\omega^{-1/2}\quad\text{for }\alpha=2\ . \tag{18c}$$

In this model both components of the complex shear viscosity show the same decay if $\alpha=2$. Note that when $\omega\tau_1\gg N^2$ (when one measures on a time scale far beyond the shortest relaxation time), $\eta''(\omega)$ decays as ω^{-1}, so the shear modulus $G'_\infty=\lim_{\omega\rightarrow\infty}\omega\eta''(\omega)$ is finite. We will use Eqs. (15) and (16) to fit the data to G_1, τ_1 and η'_∞.

III. EXPERIMENTAL

A. Synthesis of the colloidal system

The colloidal system consists of sterically stabilized silica particles dispersed in cyclohexane. The core of the particles is synthesized in a condensation polymerization reaction as described by Stöber.[30] In this reaction, tetra-ethoxy-silane $Si(OC_2H_5)_4$ is added to a solution of ammonia in ethanol. The tetra-ethoxy-silane is hydrolyzed and the product of this hydrolysis, tetra-hydroxy-silane, rapidly polymerizes to form spherical silica (SiO_2) particles. The result of this reaction is a charge-stabilized dispersion of monodisperse silica particles in ethanol. The next step is to graft a stabilizing layer of octadecyl chains on to the particle surface. This is achieved by gradually replacing the solvent ethanol by octadecyl alcohol. The obtained mixture of silica particles in octadecyl alcohol is heated for a few hours to complete the grafting reaction. The excess octadecyl alcohol is distilled off from the reaction mixture and the residue is dissolved in cyclohexane. The system is further purified by repeated centrifugation and redispersion in cyclohexane. The resulting dispersion contains sterically stabilized silica particles dissolved in cyclohexane. The preparation method was described in detail by Van Helden.[31] Larger particles can be prepared by "growing" smaller ones to the desired size.[32].

B. Particle characterization

The radius of the particles was determined with various light-scattering techniques. In the static-light-scattering (SLS) experiment the (optical) radius of gyration, which is related to the particle radius as $R_g^2=\frac{3}{5}a^2$ for a spherical optically homogeneous particle, is measured. In a dynamic-light-scattering (DLS) experiment, the diffusion coefficient, which is related to the particle radius via the Stokes-Einstein relation $D_0=k_BT/6\pi\eta_s a$, is measured.

The specific volume of the particles was determined with viscometric measurements. The relative viscosity of dilute suspensions with known weight concentration of particles was measured in an Ubbelohde capillary viscometer. These hard-sphere dispersions follow Einstein's equation for the viscosity, i.e.,

$$\eta_r=\eta/\eta_s=1+\tfrac{5}{2}\phi\ , \tag{19}$$

where ϕ is the volume fraction of the particles. The viscosity of the solvent cyclohexane is $\eta_s=0.898\times10^{-3}$ Pa s at $T=298.1$ K. The volume fraction of the particles is related to the weight concentration c via the specific volume q, $\phi=qc$. If we plot $\frac{2}{5}(\eta_r-1)$ versus c, the slope corresponds to the specific volume. In Fig. 1 this plot is shown for system SSF1. This method is discussed in more detail in Ref. 9 (see Table I).

C. Sample preparation

The concentration of a semidilute dispersion was determined by drying 5.00 ml of the stock in a dry nitrogen atmosphere. The dried silica is weighed on an analytical balance and the mass concentration is calculated. The density of the dispersion is determined also. Then a weighed amount of this characterized diluted dispersion is put into a flask of known weight. The flask is placed in a water bath. The temperature of the bath is kept at 65 °C. A weak dust-free nitrogen stream is blown over the mouth of the flask. Cyclohexane is evaporated from the sample until the desired total weight is reached. The volume fraction is then easily calculated by multiplying the concentration by the specific volume. In this way we are able to prepare very concentrated dispersions with well-defined volume fractions.

D. Description of the torsion resonators

1. *Torsion pendulums*

The simplified geometry of the instrument is shown in Fig. 2(a). Drive and detection occur through a permanent magnet inside the pendulum. The bob itself is attached to the rigid base-plate via the torsion rod. The bob is excited via two excitation coils. When a current is passed through these coils the magnet orients in the (periodic) magnetic field. In a typical experiment with a 700 Hz resonator, the angular displacement is as small as 1.5×10^{-4} rad.

The current frequency is chosen near the resonance frequency of the resonator–surrounding-fluid system, i.e.,

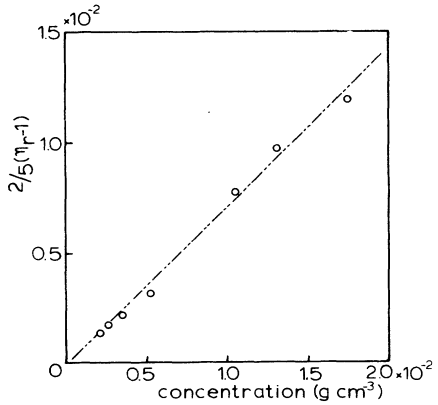

FIG. 1. Intrinsic viscosity of system SSF1.

TABLE I. Characteristic values of the model systems.

System	a (nm) (SLS)	a (nm) (DLS)	q (cm^3/g)
SP23	28±3	28±2	0.71±0.02
SSF1	48±2	46±2	0.69±0.02
SJ18	77±2	76±2	0.63±0.02

the pendulum resonance frequency. A scan is made through the resonance-frequency peak. From the broadening and the frequency shift of the resonance frequency with respect to a measurement in air, one can calculate the characteristic shear impedance of the resonator which is caused by the surrounding sample. From this impedance $Z^*(\omega)=R(\omega)+iX(\omega)$, the complex shear modulus can be calculated,

$$G^*(\omega)=G'(\omega)+iG''(\omega)=Z^{*2}(\omega)/\rho\ , \tag{20}$$

where ρ is the density of the sample. From the components of $G^*(\omega)$ the components of the complex shear viscosity can easily be calculated,

$$\eta'(\omega)=G''(\omega)/\omega,\quad \eta''(\omega)=G'(\omega)/\omega\ , \tag{21}$$

where ω is the angular resonance frequency. Since only the fundamental resonance frequency is used, each resonator gives one data point. In this study we used four pendulums with resonance frequencies of 79, 276, 709, and 2470 Hz, respectively. System SJ18 was measured at all these frequencies. All other samples were measured only at 79 and at 709 Hz.

The glass cell surrounding the resonater is double walled so that the sample and resonator can be kept at a steady temperature, namely, at 298.1±0.1 K. A detailed description of the design and the operating principle can be found in Ref. 33.

2. *Nickel-tube resonator*

The nickel-tube resonator is used to measure the complex viscosity in the frequency range 3.7–200 kHz. It

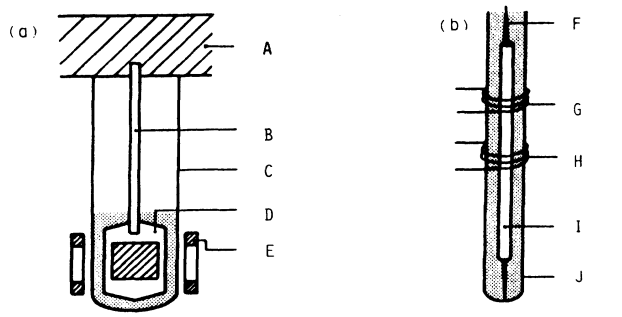

FIG. 2. Torsion resonators. (a) Torsion pendulum for measurements in the frequency range 80–2400 Hz. A, base plate; B, torsion rod; C, sample holder; D, bob with magnet inside; E, excitation and measuring coils. (b) Nickel-tube resonator for measurements in the frequency range 3.7–200 kHz. F, suspension wire; G, measuring coil; H, excitation coil; I, nickel tube; J, sample holder.

consists of a 40-cm long, circumferentially magnetized, nickel tube. This nickel tube [see Fig. 2(b)] is placed in a glass tube filled with sample. The operating and detection principle is analogous to that of the torsion pendulums. The nickel tube operates at its natural (standing torsional wave) frequency and its overtones. We measured the viscosity at ten frequencies. Again the angular displacement is very small; even at the highest frequencies the shear rate $\dot{\gamma}_{\max}$ is as low as 100 s^{-1}. The Peclet number , $\mathcal{P}=a^2\dot{\gamma}/D_0$, which expresses the competition between the disturbing effect of the shear waves and the restoring effect of the Brownian motion on the equilibrium microstructure, is small: $\mathcal{P}_{\max}=0.05$ for particles with a radius $a=50$ nm. Even at the highest frequencies, the equilibrium structure of the dispersion is perturbed slightly. The glass tube containing the resonator is placed in a thermostat bath. The temperature is constant at 298.150 within 0.002 °C. A constant temperature is required in order to prevent any change in the elasticity modulus of the nickel tube with temperature. Construction and operating details of this apparatus are described in Ref. 34. Both types of resonators require a sample volume of 18 cm^3.

E. Data collection protocol and data processing

Before each measurement on a silica dispersion, we measured the resonance frequency and bandwidth in air and in cyclohexane. For both the torsion pendulum and the nickel-tube resonator, the air measurement is necessary for calibration. The nickel-tube resonator also needs to be calibrated with a measurement on cyclohexane. Then the measuring cells were flushed with nitrogen saturated with cyclohexane. During the measurement on the sample, the nitrogen-cyclohexane atmosphere was maintained to prevent evaporation from the sample. The dispersion was measured twice. Immediately after the sample had been removed, the cell was rinsed several times with cyclohexane. Care was taken to ensure that no silica dried on the resonator surface. This is very important since a thin layer of silica on the resonator surface immediately leads to a displacement of the resonance peak and makes it impossible to reproduce the measurements. Then a cyclohexane measurement was made. If the peak positions and band widths did not correspond to the values we obtained before the sample was measured, the cell was rinsed again until the "starting" values were reproduced. Finally, the resonators were dried in a nitrogen stream.

The data (resonance peak positions and bandwidths) were stored in a microcomputer. From the displacement of the peak positions and the broadening of the peak, one can calculate the damping due to the sample. As an extra check, we calculated the complex shear viscosities from the nickel-tube-resonator data using two sets of references. We used the air and cyclohexane files which were measured before the silica dispersion was measured and compared the obtained complex shear viscosities with the values that were calculated using calibration files measured after the sample measurement. In all measurements the results agreed to within 1%.

F. Linearity checks

We checked the linearity of the measured viscoelasticity for almost every sample by doubling and halving the input voltage on the excitation coils. This operation changes the amplitude of the oscillation and thus the shear rate. The measured complex shear viscosities were found to be independent of the maximum shear rate over the full frequency range. One sample, SSF1 $\phi=0.44$, was measured with the 709-Hz resonator over almost two decades of maximum shear rate; between $\dot{\gamma}=4.57$ and 142 s^{-1} ($1.8\times10^{-3}<\mathcal{P}<5.7\times10^{-2}$). The complex shear viscosity was constant to within 1%.

More important is that we could not detect any systematic variation with increasing shear rate. The standard experiments in the torsion pendulums were performed with $\dot{\gamma}=20\ s^{-1}$.

G. Data analysis

The data were analyzed with a microcomputer. The best results were obtained when we fitted $\eta'(\omega)$ and $\eta''(\omega)$ simultaneously to Eqs. (15) and (16). In the fitting procedure, the value of τ_1 was iterated and we fitted the data to obtain G_1 and η'_∞. The number of relaxation times was set to 100. Setting the number of relaxation times to 1000 led to slightly different values for G_1 and τ_1. Even more important is the fact that the quality of the fit did not improve any further when more then a hundred relaxation times were used to describe the relaxation process (the χ^2 parameter did not change any more). Typically, we needed only six iterations. When we fitted the data for $\eta'(\omega)$ and $\eta''(\omega)$ separately, the obtained values for G_1 (and τ_1) were found to be of the same order of magnitude but could differ considerably.

In order to analyze the measurements on very concentrated samples (volume fraction $\phi>0.50$) we had to add two data points, namely, the zero-frequency low-shear value of $\eta'(\omega)$ (measured with a Deer rheometer, Deer Ltd., England) and the zero-frequency low-shear value of $\eta''(\omega)$ (which of course is zero).

IV. RESULTS AND DISCUSSION

A. Intermediate-frequency behavior

The data shown in Fig. 3 support the use of the model represented by Eqs. (17c) and (18c). All systems show the same behavior in the same dimensionless frequency region and for all volume fractions. Between $a^2\omega/D_0=1.5$ and 350, both $\eta'(\omega)$ and $\eta''(\omega)$ decay as $\omega^{-1/2}$ and can be described as

$$\eta'_r=\eta'_{r\infty}+A'(a^2\omega/D_0)^{-1/2}\ , \tag{22}$$

$$\eta''_r(\omega)=A''(a^2\omega/D_0)^{-1/2}\ . \tag{23}$$

$\eta'_r(\omega)$, $\eta''_r(\omega)$, and $\eta'_{r\infty}$ are relative viscosities (divided by the viscosity of the solvent, $\eta_s=0.898\times10^{-3}$ Pa s at $T=298.1$ K) and A' and A'' are dimensionless constants. The value of the constants A' and A'' are shown in Table II for all samples together with the slopes which

TABLE II. Dimensionless slopes A' and A'' as a function of volume fraction for three different colloidal systems in comparison with the calculated slope

$$A=(\pi/2\sqrt{2})(6\pi a^3/\eta_s k_B T)^{1/2} G_1 \tau_1^{1/2} .$$

System	ϕ	A'	A''	A
SP23	0.30	1.2±0.1	0.3±0.1	
	0.46	8.2±0.2	6.4±0.2	8.4
	0.58	47±1	45±1	60
	0.60	75±1	84±1	125
SSF1	0.42	7.9±0.7	1.1±0.2	4.7
	0.44	7.9±0.4	3.6±0.2	7.7
	0.48	12.8±0.7	5.7±0.3	12.1
	0.52	20.3±0.6	13.6±0.3	18.5
	0.54	32±1	22.7±0.5	30.6
	0.57	53±1	45.7±0.3	44.7
SJ18	0.46	6.5±0.3		6.6
	0.47	8.3±0.3	6.9±0.5	8.3
	0.51	8.1±0.4	13.6±0.2	17.9

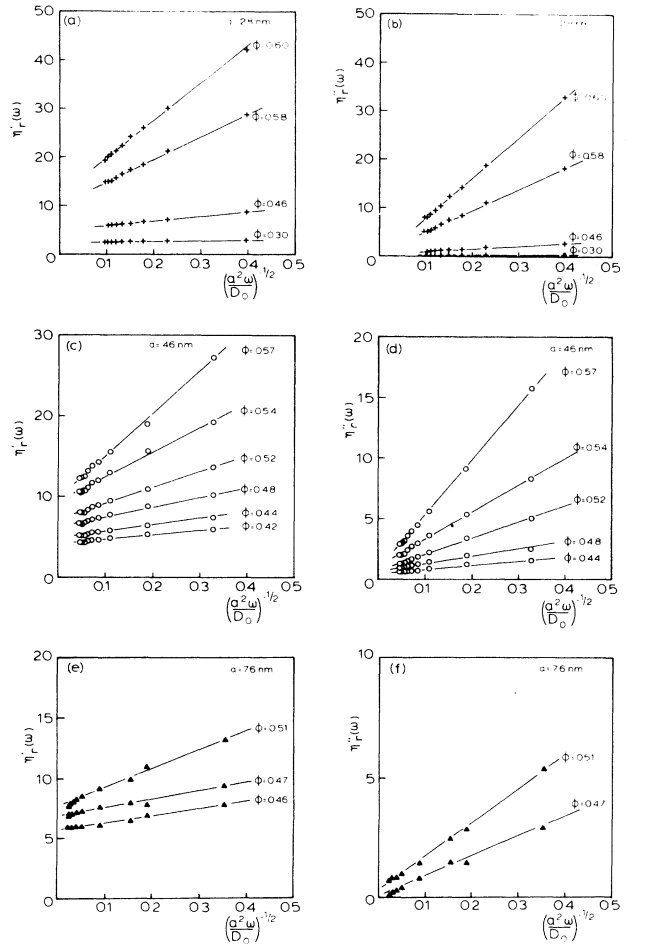

FIG. 3. Frequency dependence of the complex shear viscosity at intermediate frequencies. +, SP23; ○, SSF1; ▲, SJ18. Volume fractions as indicated. For reasons of clarity, the imaginary part of the relative complex shear viscosity $\eta_r''(\omega)$ is not shown for the samples SSF1, $\phi=0.42$ and SJ18, $\phi=0.46$.

were calculated from G_1 and τ_1 (see Sec. IV B). Note that the values of A' and A'' do not depend on the colloidal system used. But the values of A' and A'' are not equal although from the model with $\alpha=2$ one expects them to be equal. The measured and calculated slopes are not exactly the same. A'' in particular deviates systematically from the calculated value. These inconsistencies will be discussed in more detail in Sec. IV C.

B. G_1 and τ_1 as a function of particle size and volume fraction

In Fig. 4 the data are shown together with the calculated curves based on the results of the simultaneous fit to equations (15) and (16). Over the full frequency domain

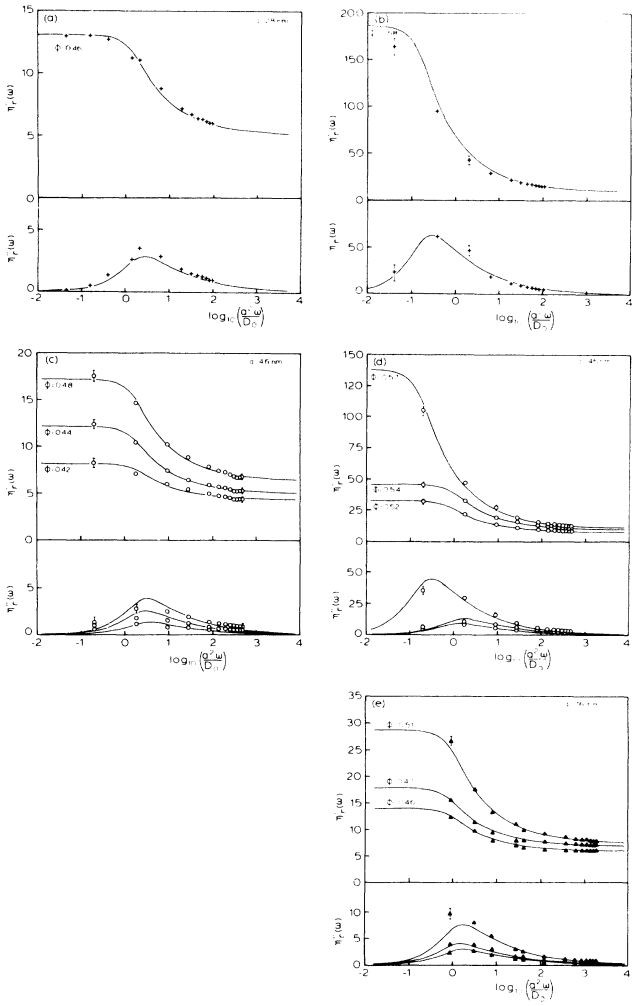

FIG. 4. Real and imaginary part of the (relative) complex shear viscosity over the full frequency range. ——, result of the fit to Eqs. (15) and (16). +, SP23; ○, SSF1; ▲, SJ18. Volume fractions as indicated in the figures. The lower parts of the figures [$\eta_r''(\omega)$] correspond to the upper halves [$\eta_r'(\omega)$]. The highest curve of $\eta_r''(\omega)$ corresponds to the highest volume fraction. The horizontal axis is the same for all figures. The result of the measurement on the most concentrated sample, SP23, $\phi=0.60$, is not shown.

and for all volume fractions the result of the fit is rather satisfactory. The numerical results for G_1, τ_1, and η'_∞ are presented in Table III.

The longest relaxation time τ_1 becomes longer with increasing volume fraction and depends on the particle size. However, the dimensionless quantity $D_0\tau_1/a^2$ is surprisingly constant for the different systems at the same volume fraction. See Fig. 5. At high volume fractions, τ_1 increases strongly with increasing volume fraction. This illustrates the dramatic slowdown of the diffusion process that is responsible for the relaxation mechanism. At $\phi=0.45$ we can compare the value of the relaxation time with experimental data on the self-diffusion coefficients of these silica particles.[22,24] Around $\phi=0.45$, the dimensionless relaxation time $D_0\tau_1/a^2=0.40-0.60$. In Sec. II, we calculated a relaxation time in a semidilute dispersion. The result was $D_0\tau_1/a^2=0.25$. Thus, at $\phi=0.45$, the relaxation is only a factor of 2 slower than in a semidilute dispersion. In such a concentrated dispersion, the average distance between the particles is very small, so short-time self-diffusion must take place over distances that are small compared to the particle radius. At $\phi=0.45$, the average distance between the particles is of the order of $0.6a$. As a characteristic time for the short-time self-diffusion, we take $t_{\text{short}}=(0.6a)^2/D_s^{\text{short}}$. Using data obtained by Van Veluwen *et al.*[22,24] we get $t_{\text{short}}=a^2/D_0$. The long-time self-diffusion takes place over distances much larger than the particle radius, for instance, over the radii of 5 particles. For this diffusion process we calculate a characteristic time as $t_{\text{long}}=(5a)^2/D_s^{\text{long}}$. In Ref. 24 we read $D_s^{\text{long}}(\phi=0.45)=0.04D_0$; this leads to $t_{\text{long}}=625a^2/D_0$. From these characteristic times, we see that the relaxation mechanism is closely connected to short-time self-diffusion. It would be interesting to normalize the volume fraction dependence of the relaxation times by scaling with the short-time self-diffusion coefficient instead of scaling with D_0. Unfortunately, no data are available for high volume fractions. As an approximation, we try to account for the slowdown of the diffusion by replacing the solvent viscosity in D_0 by the real part of the complex shear viscosity at $\omega\tau_1=1$. From the data it is found that for all volume fractions the following relation seems to hold:

$$\eta_{\text{eff}}=\eta'(\omega\tau_1=1)\cong\tfrac{2}{3}(\eta'_0-\eta'_\infty)+\eta'_\infty \ . \tag{24}$$

In Table III we show the value of the dimensionless quantity $k_BT\tau_1/6\pi\eta_{\text{eff}}a^3$ for all measured samples.

(i) This value is remarkably constant. From Table III it can be seen that G_1 varies slightly over the covered volume fraction range. It was already noted that at high volume fractions, τ_1 increases strongly with increasing volume fraction. From these observations one can conclude that it is the slow down of the diffusion that is responsible for the strong increase in the viscosity near the maximum packing fraction and not the increase of G_1. In Fig. 6 we plotted the dimensionless ratio $a^2G_1/D_0\eta_s$ as a function of volume fraction. This dimensionless ra-

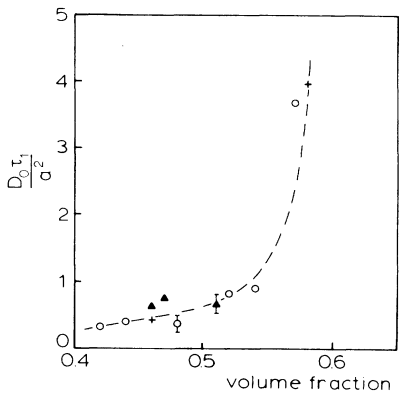

FIG. 5. Dimensionless relaxation time as a function of the volume fraction. +, SP23; ○, SSF1; ▲, SJ18. A line is drawn to guide the eye. The value of $D_0\tau_1/a^2$ at $\phi=0.60$ (12.6) is not included in the figure.

TABLE III. Results of the simultaneous fit of η' and η'' to Eqs. (15) and (16).

System	a (nm)	ϕ	G_1 (Pa)	$\frac{a^2G_1}{D_0\eta_s}$	$\frac{a^3G_1}{k_BT\phi^2}$	$\frac{\tau_1}{10^{-3}\text{ s}}$	$\frac{D_0\tau_1}{a^2}$	$\frac{\eta'_\infty}{\eta_s}$	$\frac{\eta_{\text{eff}}}{\eta_s}$	$\frac{k_BT\tau_1}{6\pi a^3\eta_{\text{eff}}}$	$\frac{(\eta'_0-\eta'_\infty)}{\eta_{\text{eff}}\phi^2}$
SP23	28	0.46	115	11.6	2.9	0.038	0.42	5.13	10.3	0.041	3.6
		0.58	270	27.2	4.3	0.36	3.97	10.0	113	0.035	4.1
		0.60	315	31.8	4.7	1.14	12.6	16.8	335	0.037	3.7
SSF1	46	0.42	16.7	7.5	2.2	0.127	0.32	4.27	7.6	0.042	3.7
		0.44	24.5	10.9	3.0	0.161	0.40	4.99	9.9	0.040	3.8
		0.48	40.0	17.9	4.1	0.149	0.37	6.36	14.4	0.026	3.7
		0.52	41.2	18.4	3.6	0.334	0.83	7.47	25.8	0.032	3.9
		0.54	61	28	5.0	0.365	0.91	9.9	39.3	0.023	3.8
		0.57	47	21	3.4	1.48	3.69	11.5	98.4	0.037	3.9
SJ18	76	0.46	3.7	7.4	1.9	1.2	0.64	5.77	11.2	0.059	3.5
		0.47	4.3	8.6	2.1	1.4	0.76	6.78	13.9	0.056	3.5
		0.51	9.7	19.5	4.0	1.2	0.68	7.45	21.1	0.031	3.8

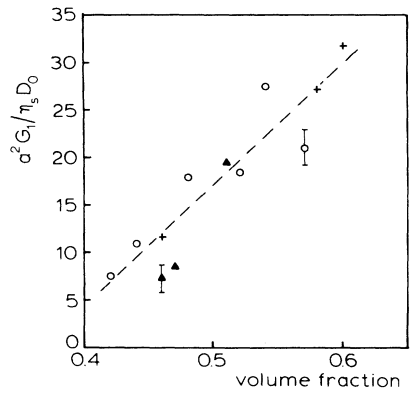

FIG. 6. Dimensionless relaxation strength as a function of the volume fraction. +, SP23; ○, SSF1; ▲, SJ18. A line is drawn to guide the eye.

tio is independent of the particle size, as was expected from the interpretation of Batchelor's theory. Although it seems as if $a^2G_1/D_0\eta_s$ is a linear function of the volume fraction, this cannot be true. G_1 must be nonzero for $\phi > 0$.

(ii) According to the model we used for the data analysis the difference $(\eta_0'-\eta_\infty')=G_1\tau_1\sum p^{-2}=(\pi^2/6)G_1\tau_1=1.65G_1\tau_1$ [see Eq. (15)]. From the data we read $(\eta_0'-\eta_\infty')/G_1\tau_1=1.7\pm0.1$.

(iii) We further noted that the ratio $(\eta_0'-\eta_\infty')/\eta_{\text{eff}}\phi^2$ appears to be independent of volume fraction and particle size (see Table III).

If the three statements (i), (ii), and (iii) do hold, then the ratio $a^3G_1/k_BT\phi^2$ should be constant. The value of this ratio is shown in Table III for all samples. As can be seen, $a^3G_1/k_BT\phi^2$ is not completely constant but varies over a factor of 2. This probably implies that the statement (i) does not hold: the dimensionless ratio $k_BT\tau_1/6\pi\eta_{\text{eff}}a^3$ is not completely independent of the volume fraction.

C. Consistency of the data analysis

In Sec. IV A we discussed the intermediate frequency behavior and concluded that the value obtained for the slopes A' and A'' did not match the predicted values of $\pi/(2\sqrt{2})G_1\tau_1^{1/2}$ completely although they were qualitatively correct. See Table II.

Of course, if the relaxation times are not spaced exactly as $\tau_p=\tau_1p^{-2}$ but as $\tau_p=\tau_1p^{-\alpha}$, with α close to 2, then the slopes A' and A'' are not equal and will be differently related to G_1 and τ_1.

In order to check whether the description can be made more consistent, we analyzed one data set (SSF1, $\phi=0.52$) with various values of α. The experimental slopes were determined by plotting $\eta'(\omega)$ and $\eta''(\omega)$ versus $(\omega)^{-1+1/\alpha}$. We further determined the values of G_1 and τ_1 as described in Sec. III G using various values for α. Using the values of G_1 and τ_1 we calculated the slopes with Eqs. (17b) and (18b). The results are shown in Table IV. It is seen that the measured slopes depend strongly on the value of α. The calculated values of A' are independent of the value of α, whereas A'' increases with increasing α. It is even more important to note that the best description is achieved using $\alpha=2$.

Therefore the remaining inconsistencies are ascribed to experimental uncertainties. Close examination of the data shows that $\eta''(\omega)$ does not decrease to zero at the highest frequencies but decays to a (very low) background. This, of course, affects the slope A''. A further decay of $\eta''(\omega)$ would increase A'' leading to a better consistency.

It should be noted that we used a simple model to analyze our data. Alternatively, the inconsistencies can be due to an inappropriate description since the model used is an *ad hoc* one.

The choice of model was based on the observed behavior at intermediate frequencies. We proposed a description in which the pth relaxation strength $G_p=G_1$ and in which $\tau_p=\tau_1p^{-2}$. At intermediate frequencies, this model leads to the expressions Eqs. (17c) and (18c). These equations suggest that if we plot $[\eta'(\omega)-\eta_\infty']/G_1\tau_1$ versus $(\omega\tau_1)^{-1/2}$, and $\eta''(\omega)/G_1\tau_1$ versus $(\omega\tau_1)^{-1/2}$, both plots are linear at intermediate frequencies and the slopes correspond to the value $\pi/(2\sqrt{2})$. In Figs. 7(a) and 7(b) we show these plots for the three different particle sizes and volume fractions ranging from 0.45 to 0.57. The lines correspond to a slope of $\pi/(2\sqrt{2})=1.11$. The result is very satisfactory and supports the proposed description of the intermediate frequency behavior.

D. High-frequency limit η_∞'

In Fig. 8 we plotted the experimental data for η_∞' together with some theoretical results. As expected, the data do not show any effect of particle size. The solid line is the result obtained by Beenakker. As discussed in Sec. II B, Beenakker's result for the high-frequency limit of the real part of the complex shear viscosity can be strictly tested with the results presented in this paper. Beenakker did not extend his calculations beyond

TABLE IV. The influence that the choice of parameter α exerts on the model parameters. Sample: SSF1, $\phi=0.52$. The value of $\alpha=2$ gives the best consistent set of parameters.

α	G_1 (Pa)	τ_1 (10^{-3} s)	A' (meas.)	A' (calc.)	A'' (meas.)	A'' (calc.)
1.67	23.2	0.56	8.1	18.6	5.4	13.5
1.82	31.5	0.40	12.7	18.6	8.5	15.9
2.00	41.2	0.33	20.2	18.6	13.5	18.6
2.22	52.3	0.29	32.4	18.6	21.6	21.4
2.40	64.8	0.25	52.2	18.6	34.9	24.3

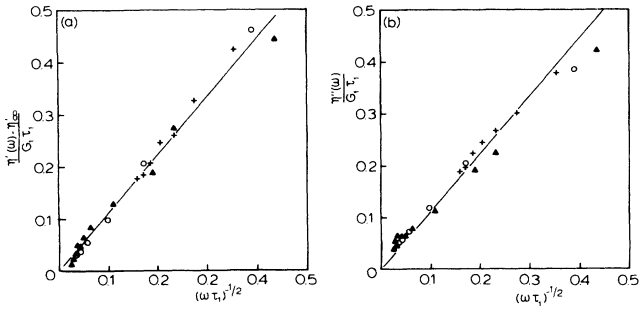

FIG. 7. Dimensionless ratio (a) $[\eta'(\omega)-\eta'_\infty]/G_1\tau_1$ and (b) $\eta''(\omega)/G_1\tau_1$ as a function of $(\omega\tau_1)^{-1/2}$. The drawn line corresponds to a slope of $\pi/(2\sqrt{2})=1.11$. +, SP23, $\phi=0.45$; ○, SSF1, $\phi=0.57$; ▲, SJ18, $\phi=0.51$.

$\phi=0.45$ because of accumulating inaccuracies. We think that the results shown in Fig. 8 are a corroboration of Beenakker's theory, and they also sustain our claim that the particles can be regarded as hard spheres. The broken line represents the result of Russel and Gast for the high shear limit of the real part of the complex shear viscosity. Their result incorporates only two-body hydrodynamic interactions since it is an extension of the theory of Batchelor and Green. The difference between their result and the result of Batchelor and Green is that Russel and Gast use a better approximation for the pair distribution function at higher volume fractions. From the data it can be seen that this two-body result describes the data only up to $\phi=0.10$ and in this volume-fraction region the Russel and Gast result essentially matches exactly the result of Batchelor and Green. The difference between the theory of Beenakker and that of Russel and Gast reflects the importance of many-body hydrodynamic interactions at higher volume fractions.

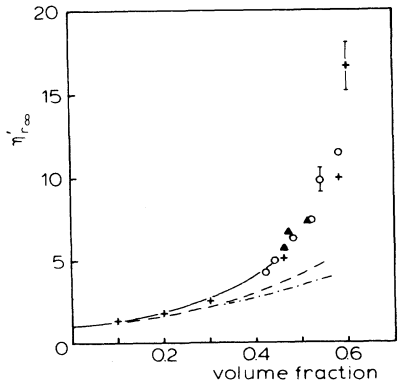

FIG. 8. High-frequency limit of the real part of the complex shear viscosity η'_∞ as a function of the volume fraction. +, SP23; ○, SSF1; ▲, SJ18. ——, Beenakker (Ref. 18); — — —, Russel and Gast (Ref. 17); —·—·—·, Batchelor and Green (Ref. 13).

E. Reduced viscosity data

From Eq. (15) it can be seen that the difference between the low- and high-shear limit of the real part of the complex shear viscosity, $\eta'_0-\eta'_\infty$, is $G_1\tau_1\sum p^{-2}=1.65G_1\tau_1$. Thus the ratio $[\eta'(\omega)-\eta'_\infty]/(\eta'_0-\eta'_\infty)$ will depend only on the dimensionless parameter $\omega\tau_1$,

$$[\eta'(\omega)-\eta'_\infty]/(\eta'_0-\eta'_\infty)=0.608\sum_{p=1}^{N}\frac{p^2}{p^4+(\omega\tau_1)^2}\ . \tag{25}$$

The imaginary term, $\eta''(\omega)$, can be reduced in the same manner,

$$\eta''(\omega)/(\eta'_0-\eta'_\infty)=0.608\sum_{p=1}^{N}\frac{\omega\tau_1}{p^4+(\omega\tau_1)^2}\ . \tag{26}$$

In Fig. 9 we plot the normalized viscosities as a function of $\omega\tau_1$. All data are brought on to the same curve. Note that the top value of $\eta''(\omega)$ is about $0.3(\eta'_0-\eta'_\infty)$, for all volume fractions, while one expects $0.5(\eta'_0-\eta'_\infty)$ for one relaxation time.

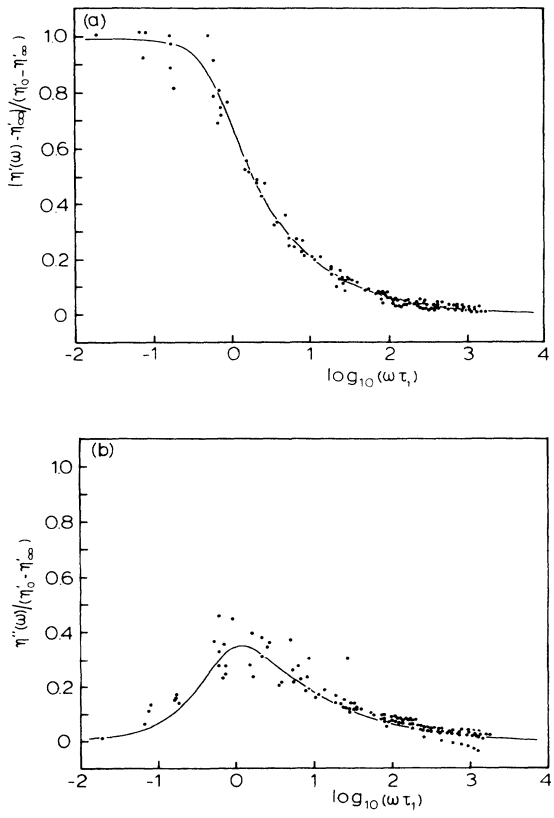

FIG. 9. Normalized complex shear viscosity as a function of $\omega\tau_1$. All data points are included. (a) Real part of the complex shear viscosity. The drawn line corresponds to $0.608\sum_{p=1}^{100}p^2/[p^4+(\omega\tau_1)^2]$. (b) The imaginary part of the complex shear viscosity. The drawn line corresponds to $0.608\sum_{p=1}^{100}\omega\tau_1/[p^4+(\omega\tau_1)^2]$.

F. Comparison of results of steady-shear measurements and of dynamical measurements

In a recent paper[9] we described steady-shear measurements on the colloidal systems SP23, SSF1, SJ18, and SJ14. Only measurements on the latter are not included in the present study. It was found that the high- and low-shear limiting viscosities, $\eta_r(\dot{\gamma}=0)$ and $\eta_r(\dot{\gamma}=\infty)$, did not depend on particle size. The low-shear limiting viscosity $\eta_r(\dot{\gamma}=0)$ is equivalent to the real part of the complex shear viscosity at $\omega=0$. The high-frequency limit η'_∞, however, cannot be compared to the high-shear limiting viscosity $\eta(\dot{\gamma}=\infty)$ since the latter is measured in a *nonlinear* experiment. In a high-shear experiment, the equilibrium microstructure of the dispersion is completely destroyed and ordering phenomena are observed.[35,36] The resulting structure is probably fully determined by hydrodynamic effects.[17]

Bedeaux[37] proposed the following formula for a sensitive representation of the relative viscosity data:

$$\frac{\eta_r-1}{\eta_r+\frac{3}{2}}=\phi[1+S(\phi)]\ , \tag{27}$$

where $S(\phi)$ is an unknown function of the volume fraction. This proposed formula is similar (in form) to the Clausius-Mossotti formula for the dielectric constant. In Fig. 10 we plotted the function $S(\phi)$ on the basis of the results of linear (dynamic) measurements of the (complex) viscosity $\eta'_{r\infty}$ and the limiting viscosities measured on system SJ18 in nonlinear (steady-shear) experiments. In this very sensitive representation of the viscosity data, the difference between the various limiting values can be seen clearly. The function $S(\phi)$ seems to be a very simple function of the volume fraction. We fitted the functions $S(\phi)$ of all dispersions to a parabola and obtained the following functions: low-shear limit (Ref. 9),

$$S(\phi)=(2.21\pm0.29)\phi-(1.47\pm0.13)\phi^2\ ;$$

high-shear limit (Ref. 9),

$$S(\phi)=(1.42\pm0.46)\phi-(0.55\pm0.35)\phi^2\ ;$$

high-frequency limit,

$$S(\phi)=(1.41\pm0.14)\phi-(1.19\pm0.34)\phi^2\ .$$

In Fig. 10 we further compared the predictions by Beenakker,[18] by Batchelor and Green,[13] and by Russel and Gast[17] with the high-frequency data. In this very sensitive representation it is seen that Beenakker's theory matches the high-frequency data rather well, in particular, at higher volume fractions. It should, however, be noted that the initial slope $S(\phi)$ according to Beenakker is too high $[S(\phi)=(2.31\pm0.14)\phi-(3.24\pm0.33)\phi^2]$. At higher volume fractions, the theory by Russel-Gast theory predicts values that are too low. Up to $\phi=0.10$, the high-frequency result of Batchelor and Green describes the data adequately. This is reflected in the value of the $O(\phi)$ coefficient of $S(\phi)$ of Russel and Gast $[S(\phi)=(0.87\pm0.21)\phi-(1.15\pm0.38)\phi^2]$, which is close to the experimental value.

In the steady-shear study,[9,10] it was further found that the shear-thinning curve, i.e., η_r as a function of the shear rate $\dot{\gamma}$, scaled with the dimensionless group $a^2\dot{\gamma}/D_0$, the so-called Peclet number. Following Krieger and Dougherty[15] we characterized the shear-thinning curve by a characteristic Peclet number $\mathcal{P}_c$, i.e., the Peclet number at which

$$\eta_r(\mathcal{P}_c)=\tfrac{1}{2}[\eta_r(\mathcal{P}\to\infty)+\eta_r(\mathcal{P}=0)]\ . \tag{28}$$

The characteristic Peclet number is an indication of the rate of deformation at which the shear thinning occurs. Both this characteristic Peclet number and τ_1 shift to lower values with increasing volume fraction. This implies that at higher volume fraction the particles need more time to rearrange in order to restore the shear-distorted particle distribution.

We can of course characterize the frequency dependence of η' by a characteristic frequency: from Fig. 9(a) can be seen that this characteristic (dimensionless) frequency $\hat{\omega}_c$ is related to τ_1 as

$$\hat{\omega}_c=1.92a^2/D_0\tau_1\ . \tag{29}$$

In Table V we compare the characteristic dimensionless frequencies and the characteristic Peclet numbers as a function of the volume fraction. Independent of the volume fraction, these characteristic times scales roughly differ by a factor of 10. The fact that the characteristic

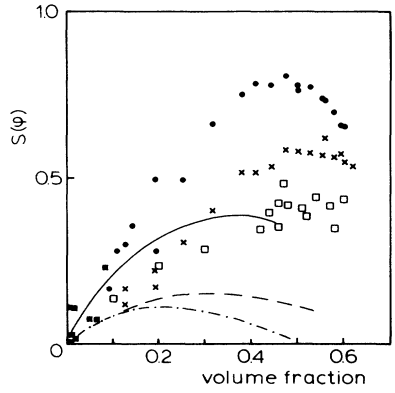

FIG. 10. Representation of various viscosity data as suggested by Bedeaux (Ref. 37). ●, SJ18 low-shear limit (Refs. 10 and 11); ×, SJ18 high-shear limit (Refs. 9 and 10); □, high-frequency limit of the real part of the complex shear viscosity (this work, Fig. 8). ——, Beenakker (Ref. 18); — — —, Russel and Gast (Ref. 17); —·—·—·, Batchelor and Green (Ref. 13).

TABLE V. A comparison of characteristic Peclet numbers (Ref. 9) and characteristic dimensionless frequencies (see Fig. 5 and Table III).

ϕ	$\mathcal{P}_c$	$\hat{\omega}_c$
0.40	0.9	8
0.45	0.6	4
0.50	0.4	3
0.55	0.14	1.3

Peclet number is smaller than the characteristic dimensionless frequency reflects the nonlinearity of the steady-shear experiment. In a steady-shear experiment (at higher Peclet numbers) the micro structure is brought far out of equilibrium and particles have to diffuse over longer distances in order to restore the equilibrium distribution. In a linear experiment, short-time self-diffusion restores equilibrium. In the nonlinear case another type of diffusion takes care of the restoration of the particle distribution. Short-time self-diffusion is faster than all other diffusion processes.[22,24] We think it is for this reason that the shear thinning in a nonlinear experiment becomes noticeable at a longer time scale, thus at a lower Peclet number.

V. CONCLUSIONS

We measured the *linear* viscoelastic behavior of hard-sphere colloidal dispersions as a function of frequency, particle size, and volume fraction. Guided by the observed behavior of the complex shear viscosity at intermediate frequencies, we chose a simple model to describe the data. The three important model parameters (the relaxation strength G_1, the longest relaxation time τ_1, and the high-frequency limit of the real part of the complex viscosity η'_∞) were determined.

It was shown that irrespective of the particle size the complex shear viscosity can be described with the dimensionless parameters $a^2G_1/D_0\eta_s$ and $D_0\tau_1/a^2$. This scaling behavior was already predicted by the theory of Batchelor and Green. The longest relaxation time τ_1 increases with increasing volume fraction. This implies that the diffusion which is responsible for the relaxation mechanism slows down with increasing volume fraction. This observation, and values of τ_1, strongly support the point of view that the diffusion process of interest is closely connected with the short-time self-diffusion.

From the Russel–Gast theory we calculated a mean relaxation time as a function of volume fraction. The experiments show that this mean relaxation time increases with increasing volume fraction, whereas Russel and Gast predict a decrease of the mean relaxation time.

We tried to normalize τ_1 by replacing the solvent viscosity in D_0 by an effective viscosity. In this way we tried to account for the slowdown of the diffusion. The obtained values for the normalized τ_1 were found to be almost independent of volume fraction. The dimensionless relaxation strength, i.e., $a^2G_1/D_0\eta_s$, was also found to be independent of particle size.

At higher volume fractions, the high-frequency limit η'_∞ matches the calculations of Beenakker which are based on many-body hydrodynamic interactions. Russel and Gast treat the hydrodynamics at the pair level. This results in too low a value for η'_∞. Up to $\phi=0.10$, the high-frequency data can be described with the high-frequency result of Batchelor and Green.

With the obtained values for τ_1 and η'_∞, we normalized the complex shear viscosity. Data for all volume fractions can be brought onto the same curve.

ACKNOWLEDGMENTS

Miss Petri Mast is thanked for assisting with the measurements on SSF1 and SP23. We thank Mr. Rob van der Hoeven for his assistance in analyzing the data. We thank Professor H. N. W. Lekkerkerker and Dr. J. K. G. Dhont for discussing important issues with us. This work is part of the research program of the Foundation for Research on Matter with financial support from the Netherlands Organization for Pure Research.

[1]D. W. Benzing and W. B. Russel, J. Colloid Interface Sci. **83**, 163 (1981).
[2]C. Blom, J. Mellema, J. S. Lopulissa, and A. J. Reuvers, Colloid Polym. Sci. **262**, 397 (1984).
[3]G. Schoukens and J. Mewis, J. Rheol. **22**, 381 (1978).
[4]J. G. Goodwin, R. W. Hughes, S. J. Partridge, and C. Zukoski, J. Chem. Phys. **85**, 559 (1986).
[5]M. Oosterbroek, J. Mellema, and J. S. Lopulissa, J. Colloid Interface Sci. **84**, 14 (1981).
[6]C. Blom and J. Mellema, J. Disp. Sci. Techn. **5**, 193 (1984).
[7]A. Vrij, J. W. Jansen, J. K. G. Dhont, C. Pathmamanoharan, M. M. Kops-Werkhoven, and H. M. Fijnaut, Faraday Discuss. Chem. Soc. **76**, 19 (1983).
[8]C. G. de Kruif, W. J. Briels, R. P. May, and A. Vrij, Langmuir **4**, 668 (1988).
[9]J. C. van der Werff and C. G. de Kruif, J. Rheol. (to be published).
[10]C. G. de Kruif, E. M. F. van Iersel, A. Vrij, and W. B. Russel, J. Chem. Phys. **83**, 4717 (1985).
[11]A. Einstein, in *Investigations on the Theory of the Brownian Movement*, edited by R. Furth (Dover, New York, 1956).
[12]G. K. Batchelor, J. Fluid Mech. **41**, 545 (1970).
[13]G. K. Batchelor and J. T. Green, J. Fluid Mech. **56**, 401 (1972).
[14]G. K. Batchelor, J. Fluid Mech. **83**, 97 (1977).
[15]I. M. Krieger and T. J. Dougherty, Trans. Soc. Rheol. **3**, 137 (1959).
[16]J. Mellema, C. G. de Kruif, C. Blom, and A. Vrij, Rheol. Acta **26**, 40 (1987).
[17]W. B. Russel and A. P. Gast, J. Chem. Phys. **84**, 1815 (1986).
[18]C. W. J. Beenakker, Physica **128A**, 48 (1984).
[19]It was shown by Dhont that the Smoluchowski equation that $g(r)$ has to obey is singularly perturbed. As a result, $g(r)$ is not analytic in the shear rate. Strictly speaking, Eq. (2) is not correct. It can be shown, however, that for the calculation of ensemble averages, such as the effective stress tensor, at very low shear rates, Eq. (2) yields good approximations [J. K. G. Dhont, Physica **146**, 541 (1987)].
[20]C. W. J. Beenakker and P. Mazur, Phys. Lett. A **98**, 22 (1983).
[21]C. W. J. Beenakker and P. Mazur, Physica **126A**, 349 (1984).
[22]A. van Veluwen, H. N. W. Lekkerkerker, C. G. de Kruif, and A. Vrij, Faraday Discuss. Chem. Soc. **83**, 59 (1987).
[23]P. N. Pusey and W. van Megen, J. Phys. (Paris) **44**, 258 (1983).
[24]A. van Veluwen, Ph. D. dissertation, Utrecht, 1987.
[25]T. S. Lundgren, J. Fluid Mech. **51**, 273 (1972).
[26]D. Bedeaux, Physica **121A**, 345 (1983).
[27]J. Mellema and M. W. M. Willemse, Physica **122A**, 286 (1983).
[28]B. Cichocki and B. U. Felderhof, J. Chem. Phys. **89**, 1049

(1988).
[29]J. D. Ferry, *Viscoelastic Properties of Polymers* (Wiley, New York, 1970).
[30]W. Stöber, A. Fink, and E. Bohn, J. Colloid Interface Sci. **26**, 62 (1968).
[31]A. K. van Helden, J. W. Jansen, and A. Vrij, J. Colloid Interface Sci. **81**, 354 (1981).
[32]S. Coehen and C. de Kruif, J. Colloid Interface Sci. **124**, 104 (1900).
[33]C. Blom, J. Mellema, Rheol. Acta **23**, 98 (1984).
[34]M. Oosterbroek, H. A. Waterman, S. S. Wiseall, E. G. Altena, J. Mellema, and G. A. M. Kip, Rheol. Acta **19**, 497 (1980).
[35]B. J. Ackerson, J. C. van der Werff, and C. G. de Kruif, Phys. Rev. A **37**, 4819 (1988).
[36]S. J. Johnson and C. G. de Kruif, J. Chem. Phys. (to be published).
[37]D. Bedeaux, J. Colloid Interface Sci. **118**, 80 (1987).